Integral Line-of-Sight for path following of underwater snake robots

E. Kelasidi, K. Y. Pettersen, P. Liljebäck and J. T. Gravdahl

Abstract— **This paper considers straight line path following control of underwater snake robots in the presence of constant irrotational currents. An integral line-of-sight (LOS) guidance law is proposed, which is combined with a sinusoidal gait pattern and a directional controller that steers the robot towards and along the desired path. Integral action is introduced in the guidance law to compensate for the ocean current effect. The stability of the proposed control scheme in the presence of ocean currents is investigated. In particular, using Poincaré map analysis, we prove that the state variables of an underwater snake robot trace out an exponentially stable periodic orbit when the integral LOS path following controller is applied. Simulation results are presented to illustrate the performance of the proposed path following controller for both lateral undulation and eel-like motion.**

I. Introduction

For centuries, engineers and scientists have gained inspiration from the natural world in their search for solutions to technical problems, and this process is termed biomimetics. Underwater snake robots have several promising applications for underwater exploration, monitoring, surveillance and inspection. They thus bring a promising prospective to improve the efficiency and maneuverability of modern-day underwater vehicles. These mechanisms carry a lot of potential for inspection of subsea oil and gas installations. Also, for the biological community and marine archeology, snake robots that are able to swim smoothly without much noise, and that can navigate in difficult environments such as ship wrecks, are very interesting [1]. To realize operational snake robots for such underwater applications, a number of different control design challenges must first be solved. An important control problem concerns the ability to follow given reference paths under the influence of ocean current effects, and this is the topic of this paper.

Studies of hyper-redundant mechanisms (HRMs) have largely restricted themselves to land-based studies, while several models for snake robots have been proposed [2]. Empirical and analytic studies of snake locomotion were reported by Gray [3], while the work of Hirose [4] is among the first attempts to develop a snake robot prototype. Comparing amphibious snake robots to the traditional land-based ones, the former have the advantage of adaptability to aquatic environments. Research on amphibious snake robots (also referred to as lamprey robots or eel-like robots) is, however, much less extensive than for the traditional types and fewer prototypes have been developed [5], [6]. Several results have been reported in the related field of design, modeling and control of underwater robots that mimic the movement of fish [7]. Regarding swimming snake robots, the underlying propulsive force generation mechanism has been studied through exploration of the fluid dynamics surrounding the body. In this field, several mathematical models of underwater snake robots have been proposed [1], [8], [9], [10], [11], [12], [13], [14].

Several control approaches for underwater snake robots have been proposed in the literature. However, the emphasis so far has mainly been on achieving forward and turning locomotion [8]. The next step would be not only to achieve forward locomotion, but also to make the snake robot follow a desired path, i.e. solving the path following control problem. The works of [8], [15] and [16] synthesize gaits for translational and rotational motion of various fish-like mechanisms and propose controllers for tracking straight and curved trajectories. The work of [17] study the evolution from fish to amphibian by use of central pattern generators (CPG). Eel-like motion is considered in [8] and [18], where controllers for tracking straight and curved trajectories are proposed. Previous approaches for path following control are based on dynamic models of the swimming robots where ocean current effects are neglected.

In [1], the authors propose a model of underwater snake robots, where the dynamic equations are written in closed form. This modeling approach takes into account both the linear and the nonlinear drag forces (resistive fluid forces), the added mass effect (reactive fluid forces), the fluid moments and current effects. Based on the dynamic model presented in [1], we propose in this paper an integral line-of-sight path following controller for steering an underwater snake robot along a straight line path in the presence of ocean currents. The integral LOS guidance law is inspired by path following control of marine surface vessels in the presence of ocean currents [19], [20]. Note that the integral LOS guidance strategy is widely used for directional control of marine surface vessels for ocean current compensation but has, to our best knowledge, not been employed previously for directional control of underwater snake robots in the presence of ocean currents.

The method of Poincaré maps is a widely used tool for studying the stability of periodic solutions in dynamical

J. T. Gravdahl is with the Dept. of Engineering Cybernetics at NTNU, NO-7491 Trondheim, Norway. E-mail: Tommy.Gravdahl@itk.ntnu.no

E. Kelasidi, and K. Y. Pettersen are with the Centre for Autonomous Marine Operations and Systems, Dept. of Engineering Cybernetics at NTNU, NO-7491 Trondheim, Norway. E-mail: {Eleni.Kelasidi,Kristin.Y.Pettersen}@itk.ntnu.no

Affiliation of P. Liljebäck is shared between the Dept. of Engineering Cybernetics at NTNU, NO-7491 Trondheim, Norway, and SINTEF ICT, Dept. of Applied Cybernetics, N-7465 Trondheim, Norway. E-mail: Pal.Liljeback@sintef.no.

This work was partly supported by the Research Council of Norway through project no. 205622 and its Centres of Excellence funding scheme, project no. 223254-AMOS

systems. Poincaré maps are employed in [2], [21] to study the stability properties of ground snake robot locomotion. Motivated by this work, we analyse the stability of the locomotion of an underwater snake robot along the straight line path in the presence of ocean currents using a Poincaré map. In particular, by using a Poincaré map, we prove that all state variables of an underwater snake robot, except the position along the forward direction, trace out an exponentially stable periodic orbit when the integral LOS path following controller is applied. To the authors' best knowledge, no formal stability analysis of an integral LOS path following controller for an underwater snake robot has been presented in previous literature.

The paper is organized as follows. Section II presents the dynamic model of an underwater snake robot, while the integral line-of-sight path following controller along straight lines is outlined in Section III. The stability analysis based on the Poincaré map approach is presented in Section IV, followed by simulation results for both lateral undulation and eel-like motion in Section V. Finally, conclusions and suggestions for further research are given in Section VI.

II. Dynamic Modeling of Underwater Snake Robots

This section briefly presents a model of the kinematics and dynamics of an underwater snake robot moving in a virtual horizontal plane. A more detailed presentation of the model is given in [1].

A. Notations and defined symbols

The underwater snake robot consists of n rigid links of equal length $2l$ interconnected by $n-1$ joints. The links are assumed to have the same mass m and moment of inertia $J=\frac{1}{3}ml^2$. The mass of each link is uniformly distributed so that the link CM (center of mass) is located at its center point (at length l from the joint at each side). The total mass of the snake robot is therefore nm. In the following sections, the kinematics and dynamics of the robot will be described in terms of the mathematical symbols described in Table I and illustrated in Fig. 1. The following vectors and matrices are used in the subsequent sections:

$$\mathbf{A}=\begin{bmatrix} 1 & 1 & & \\ & \ddots & \ddots & \\ & & 1 & 1 \end{bmatrix}, \mathbf{D}=\begin{bmatrix} 1 & -1 & & \\ & \ddots & \ddots & \\ & & 1 & -1 \end{bmatrix},$$

where $\mathbf{A},\mathbf{D}\in\mathbb{R}^{(n-1)\times n}$. Furthermore,

$$\mathbf{e}=\begin{bmatrix} 1 & \dots & 1 \end{bmatrix}^T\in\mathbb{R}^n, \mathbf{E}=\begin{bmatrix} \mathbf{e} & \mathbf{0}_{n\times 1} \\ \mathbf{0}_{n\times 1} & \mathbf{e} \end{bmatrix}\in\mathbb{R}^{2n\times 2},$$

$$\sin\theta = \begin{bmatrix} \sin\theta_1 & \dots & \sin\theta_n \end{bmatrix}^T\in\mathbb{R}^n, \mathbf{S}_\theta=\mathrm{diag}(\sin\theta)\in\mathbb{R}^{n\times n},$$

$$\cos\theta = \begin{bmatrix} \cos\theta_1 & \dots & \cos\theta_n \end{bmatrix}^T\in\mathbb{R}^n, \mathbf{C}_\theta=\mathrm{diag}(\cos\theta)\in\mathbb{R}^{n\times n}$$

$$\mathrm{sgn}\theta = \begin{bmatrix} \mathrm{sgn}\theta_1 & \dots & \mathrm{sgn}\theta_n \end{bmatrix}^T\in\mathbb{R}^n$$

$$\dot\theta^2 = \begin{bmatrix} \dot\theta_1{}^2 & \dots & \dot\theta_n{}^2 \end{bmatrix}^T\in\mathbb{R}^n, \mathbf{J}=J\mathbf{I}_n, \mathbf{L}=l\mathbf{I}_n, \mathbf{M}=m\mathbf{I}_n$$

$$\mathbf{K}=\mathbf{A}^T\left(\mathbf{D}\mathbf{D}^T\right)^{-1}\mathbf{D}, \mathbf{V}=\mathbf{A}^T\left(\mathbf{D}\mathbf{D}^T\right)^{-1}\mathbf{A}$$

B. Kinematics of the underwater snake robot

The snake robot is assumed to move in a virtual horizontal plane, fully immersed in water, and has n+2 degrees of freedom (n links angles and the x-y position of the robot). The *link angle* of each link $i\in 1,\dots,n$ of the snake robot is denoted by $\theta_i\in\mathbb{R}$, while the *joint angle* of joint $i\in 1,\dots,n-1$ is given by $\phi_i=\theta_i-\theta_{i-1}$. The *heading* (or *orientation*) $\bar\theta\in\mathbb{R}$ of the snake is defined as the average of the link angles, i.e. as [2]

$$\bar\theta=\frac{1}{n}\sum_{i=1}^{n}\theta_i. \tag{1}$$

The global frame position $\mathbf{p}_{\mathrm{CM}}\in\mathbb{R}^2$ of the CM (center of mass) of the robot is given by

$$\mathbf{p}_{\mathrm{CM}}=\begin{bmatrix} p_x \\ p_y \end{bmatrix}=\begin{bmatrix} \frac{1}{nm}\sum_{i=1}^{n} mx_i \\ \frac{1}{nm}\sum_{i=1}^{n} my_i \end{bmatrix}=\frac{1}{n}\begin{bmatrix} \mathbf{e}^T\mathbf{X} \\ \mathbf{e}^T\mathbf{Y} \end{bmatrix}, \tag{2}$$

where (x_i,y_i) are the global frame coordinates of the CM of link i, $\mathbf{X}=[x_1,\dots,x_n]^T\in\mathbb{R}^n$ and $\mathbf{Y}=[y_1,\dots,y_n]^T\in\mathbb{R}^n$. The forward velocity of the robot is denoted by $\bar v_t\in\mathbb{R}$ and is defined as the component of the CM velocity along the current heading of the snake, i.e.

$$\bar v_t=\dot p_x\cos\bar\theta+\dot p_y\sin\bar\theta. \tag{3}$$

The links are constrained by the joints according to

$$\mathbf{D}\mathbf{X}+l\mathbf{A}\cos\theta=\mathbf{0}, \quad \mathbf{D}\mathbf{Y}+l\mathbf{A}\sin\theta \quad =\mathbf{0}. \tag{4}$$

It is shown in [1] that the position of the individual links as a function of the CM position and the link angles is given by

$$\mathbf{X}=-l\mathbf{K}^T\cos\theta+\mathbf{e}p_x, \qquad \mathbf{Y}=-l\mathbf{K}^T\sin\theta+\mathbf{e}p_y, \tag{5}$$

where $\mathbf{K}=\mathbf{A}^T\left(\mathbf{D}\mathbf{D}^T\right)^{-1}\mathbf{D}\in\mathbb{R}^{n\times n}$, and where $\mathbf{D}\mathbf{D}^T$ is nonsingular and thereby invertible [2]. The linear velocities of the links are given by

$$\dot{\mathbf{X}}=l\mathbf{K}^T\mathbf{S}_\theta\dot\theta+\mathbf{e}\dot p_x, \quad \dot{\mathbf{Y}}=-l\mathbf{K}^T\mathbf{C}_\theta\dot\theta+\mathbf{e}\dot p_y. \tag{6}$$

The linear accelerations of the links are found by differentiating the velocity of the individual links (6) with respect to time, which gives

$$\ddot{\mathbf{X}}=l\mathbf{K}^T\left(\mathbf{C}_\theta\dot\theta^2+\mathbf{S}_\theta\ddot\theta\right)+\mathbf{e}\ddot p_x, \quad \ddot{\mathbf{Y}}=l\mathbf{K}^T\left(\mathbf{S}_\theta\dot\theta^2-\mathbf{C}_\theta\ddot\theta\right)+\mathbf{e}\ddot p_y. \tag{7}$$

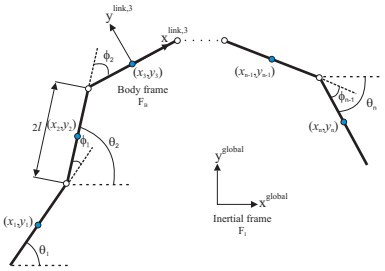

(a) Kinematic parameters

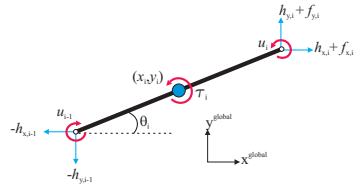

(b) Forces and torques acting on each link

Fig. 1: Underwater snake robot

TABLE I: Definition of mathematical terms

Symbol	Description	Vector
n	The number of links	
l	The half length of a link	
m	Mass of each link	
J	Moment of inertia of each link	
θ_i	Angle between link i and the global x axis	$\theta\in\mathbb{R}^n$
ϕ_i	Angle of joint i	$\phi\in\mathbb{R}^{n-1}$
(x_i,y_i)	Global coordinates of the CM of link i	$\mathbf{X},\mathbf{Y}\in\mathbb{R}^n$
(p_x,p_y)	Global coordinates of the CM of the robot	$\mathbf{p}_{CM}\in\mathbb{R}^2$
u_i	Actuator torque of joint between link i and link $i+1$	$\mathbf{u}\in\mathbb{R}^{n-1}$
u_{i-1}	Actuator torque of joint between link i and link $i-1$	$\mathbf{u}\in\mathbb{R}^{n-1}$
$(f_{x,i},f_{y,i})$	Fluid force on link i	$\mathbf{f}_x,\mathbf{f}_y\in\mathbb{R}^n$
τ_i	Fluid torque on link i	$\tau\in\mathbb{R}^n$
$(h_{x,i},h_{y,i})$	Joint constraint force on link i from link $i+1$	$\mathbf{h}_x,\mathbf{h}_y\in\mathbb{R}^{n-1}$
$-(h_{x,i-1},h_{y,i-1})$	Joint constraint force on link i from link $i-1$	$\mathbf{h}_x,\mathbf{h}_y\in\mathbb{R}^{n-1}$

Note that in this paper (7) has been adjusted compared to the corresponding expression presented in [1] in order to express the acceleration of the links in a more proper way, by also taking into account the acceleration of the CM.

C. Hydrodynamic modeling

As has been noted in the bio-robotics community, underwater snake (eel-like) robots bring a promising prospective to improve the efficiency and maneuverability of modern-day underwater vehicles. The dynamic modeling of the contact forces is, however, quite complicated compared to the modeling of the overall rigid motion. The hydrodynamic modeling approach from [1] that is considered in this paper, takes into account both the linear and the nonlinear drag forces (resistive fluid forces), the added mass effect (reactive fluid forces), the fluid moments and current effects. In particular, in [1] it is shown that the fluid forces on all links can be expressed in vector form as

$$\mathbf{f} = \begin{bmatrix} \mathbf{f_x} \\ \mathbf{f_y} \end{bmatrix} = \begin{bmatrix} \mathbf{f_{A_x}} \\ \mathbf{f_{A_y}} \end{bmatrix} + \begin{bmatrix} \mathbf{f^I_{D_x}} \\ \mathbf{f^I_{D_y}} \end{bmatrix} + \begin{bmatrix} \mathbf{f^{II}_{D_x}} \\ \mathbf{f^{II}_{D_y}} \end{bmatrix}. \tag{8}$$

The vectors $\mathbf{f_{A_x}}$ and $\mathbf{f_{A_y}}$ represent the effects from added mass forces and are expressed as

$$\begin{aligned} \begin{bmatrix} \mathbf{f_{A_x}} \\ \mathbf{f_{A_y}} \end{bmatrix} &= -\begin{bmatrix} \mu_n(\mathbf{S}_\theta)^2 & -\mu_n\mathbf{S}_\theta\mathbf{C}_\theta \\ -\mu_n\mathbf{S}_\theta\mathbf{C}_\theta & \mu_n(\mathbf{C}_\theta)^2 \end{bmatrix} \begin{bmatrix} \ddot{\mathbf{X}} \\ \ddot{\mathbf{Y}} \end{bmatrix} \\ &\quad -\begin{bmatrix} -\mu_n\mathbf{S}_\theta\mathbf{C}_\theta & -\mu_n(\mathbf{S}_\theta)^2 \\ \mu_n(\mathbf{C}_\theta)^2 & \mu_n\mathbf{S}_\theta\mathbf{C}_\theta \end{bmatrix} \begin{bmatrix} \mathbf{V}_x^a \\ \mathbf{V}_y^a \end{bmatrix} \dot{\theta}, \end{aligned} \tag{9}$$

where $\mathbf{V}_x^a = \text{diag}(V_{x,1},\ldots,V_{x,n}) \in \mathbb{R}^{n\times n}$, $\mathbf{V}_y^a = \text{diag}(V_{y,1},\ldots,V_{y,n}) \in \mathbb{R}^{n\times n}$ and $[V_{x,i}, V_{y,i}]^T$ is the current velocity expressed in inertial frame coordinates. The vectors $\mathbf{f^I_{D_x}}$, $\mathbf{f^I_{D_y}}$ and $\mathbf{f^{II}_{D_x}}$, $\mathbf{f^{II}_{D_y}}$ present the effects from the linear (10) and nonlinear drag forces (11), respectively, where the relative velocities are given by (12).

$$\begin{bmatrix} \mathbf{f^I_{D_x}} \\ \mathbf{f^I_{D_y}} \end{bmatrix} = -\begin{bmatrix} c_t(\mathbf{C}_\theta)^2 + c_n(\mathbf{S}_\theta)^2 & (c_t - c_n)\mathbf{S}_\theta\mathbf{C}_\theta \\ (c_t - c_n)\mathbf{S}_\theta\mathbf{C}_\theta & c_t(\mathbf{S}_\theta)^2 + c_n(\mathbf{C}_\theta)^2 \end{bmatrix} \begin{bmatrix} \dot{\mathbf{X}} - \mathbf{V}_x \\ \dot{\mathbf{Y}} - \mathbf{V}_y \end{bmatrix} \tag{10}$$

$$\begin{bmatrix} \mathbf{f^{II}_{D_x}} \\ \mathbf{f^{II}_{D_y}} \end{bmatrix} = -\begin{bmatrix} c_t\mathbf{C}_\theta & -c_n\mathbf{S}_\theta \\ c_t\mathbf{S}_\theta & c_n\mathbf{C}_\theta \end{bmatrix} \text{sgn}\left(\begin{bmatrix} \mathbf{V_{r_x}} \\ \mathbf{V_{r_y}} \end{bmatrix}\right) \begin{bmatrix} \mathbf{V_{r_x}}^2 \\ \mathbf{V_{r_y}}^2 \end{bmatrix} \tag{11}$$

$$\begin{bmatrix} \mathbf{V_{r_x}} \\ \mathbf{V_{r_y}} \end{bmatrix} = \begin{bmatrix} \mathbf{C}_\theta & \mathbf{S}_\theta \\ -\mathbf{S}_\theta & \mathbf{C}_\theta \end{bmatrix} \begin{bmatrix} \dot{\mathbf{X}} - \mathbf{V}_x \\ \dot{\mathbf{Y}} - \mathbf{V}_y \end{bmatrix} \tag{12}$$

In addition, the fluid torques on all links are

$$\tau = -\Lambda_1\ddot{\theta} - \Lambda_2\dot{\theta} - \Lambda_3\dot{\theta}|\dot{\theta}|, \tag{13}$$

where $\Lambda_1 = \lambda_1\mathbf{I}_n$, $\Lambda_2 = \lambda_2\mathbf{I}_n$ and $\Lambda_3 = \lambda_3\mathbf{I}_n$. The coefficients c_t, c_n, λ_2, λ_3 represent the drag forces parameters due to the pressure difference between the two sides of the body, and the parameters μ_n, λ_1 represent the added mass of the fluid carried by the moving body.

D. Equations of motion

This section presents the equations of motion for the underwater snake robot. In [1], it is shown that the force balance equations for all links may be expressed in matrix form as

$$m\ddot{\mathbf{X}} = \mathbf{D}^T\mathbf{h}_x + \mathbf{f_x}, \quad m\ddot{\mathbf{Y}} = \mathbf{D}^T\mathbf{h}_y + \mathbf{f_y}. \tag{14}$$

Note that the link accelerations may also be expressed by differentiating (4) twice with respect to time. This gives

$$\mathbf{D}\ddot{\mathbf{X}} = l\mathbf{A}\left(\mathbf{C}_\theta\dot{\theta}^2 + \mathbf{S}_\theta\ddot{\theta}\right), \quad \mathbf{D}\ddot{\mathbf{Y}} = l\mathbf{A}\left(\mathbf{S}_\theta\dot{\theta}^2 - \mathbf{C}_\theta\ddot{\theta}\right). \tag{15}$$

We obtain the acceleration of the CM by differentiating (2) twice with respect to time, inserting (14), and noting that the constraint forces $\mathbf{h}_x$ and $\mathbf{h}_y$, are cancelled out when the link accelerations are summed. This gives

$$\begin{bmatrix} \ddot{p}_x \\ \ddot{p}_y \end{bmatrix} = \frac{1}{n}\begin{bmatrix} \mathbf{e}^T\ddot{\mathbf{X}} \\ \mathbf{e}^T\ddot{\mathbf{Y}} \end{bmatrix} = \frac{1}{nm}\begin{bmatrix} \mathbf{e}^T & \mathbf{0}_{1\times n} \\ \mathbf{0}_{1\times n} & \mathbf{e}^T \end{bmatrix}\mathbf{f} \tag{16}$$

By inserting (7), (8) and (9) into (16) the acceleration of the CM may be expressed as

$$\begin{aligned} \begin{bmatrix} \ddot{p}_x \\ \ddot{p}_y \end{bmatrix} &= -\mathbf{M}_p\begin{bmatrix} \mathbf{e}^T\mu_n\mathbf{S}_\theta^2 & -\mathbf{e}^T\mu_n\mathbf{S}_\theta\mathbf{C}_\theta \\ -\mathbf{e}^T\mu_n\mathbf{S}_\theta\mathbf{C}_\theta & \mathbf{e}^T\mu_n\mathbf{C}_\theta^2 \end{bmatrix}\begin{bmatrix} l\mathbf{K}^T(\mathbf{C}_\theta\dot{\theta}^2 + \mathbf{S}_\theta\ddot{\theta}) \\ l\mathbf{K}^T(\mathbf{S}_\theta\dot{\theta}^2 - \mathbf{C}_\theta\ddot{\theta}) \end{bmatrix} \\ &\quad -\mathbf{M}_p\begin{bmatrix} -\mathbf{e}^T\mu_n\mathbf{S}_\theta\mathbf{C}_\theta & -\mathbf{e}^T\mu_n\mathbf{S}_\theta^2 \\ \mathbf{e}^T\mu_n\mathbf{C}_\theta^2 & \mathbf{e}^T\mu_n\mathbf{S}_\theta\mathbf{C}_\theta \end{bmatrix}\begin{bmatrix} \mathbf{V}_x^a \\ \mathbf{V}_y^a \end{bmatrix}\dot{\theta} + \mathbf{M}_p\begin{bmatrix} \mathbf{e}^T\mathbf{f_{Dx}} \\ \mathbf{e}^T\mathbf{f_{Dy}} \end{bmatrix} \end{aligned} \tag{17}$$

where

$$\mathbf{M}_p = \begin{bmatrix} m_{11} & m_{12} \\ m_{21} & m_{22} \end{bmatrix} = \begin{bmatrix} nm + \mathbf{e}^T\mu_n\mathbf{S}_\theta^2\mathbf{e} & -\mathbf{e}^T\mu_n\mathbf{S}_\theta\mathbf{C}_\theta\mathbf{e} \\ -\mathbf{e}^T\mu_n\mathbf{S}_\theta\mathbf{C}_\theta\mathbf{e} & nm + \mathbf{e}^T\mu_n\mathbf{C}_\theta^2\mathbf{e} \end{bmatrix}^{-1}. \tag{18}$$

and $\mathbf{f_{Dx}} = \mathbf{f^I_{D_x}} + \mathbf{f^{II}_{D_x}}$ and $\mathbf{f_{Dy}} = \mathbf{f^I_{D_y}} + \mathbf{f^{II}_{D_y}}$ are the drag forces in x and y directions. Additionally, it is easily verifiable that the determinant $n^2m^2 + nm\mu_n + \mu_n^2\sum_{i=1}^{n-1}\sum_{j=i+1}^{n}(\sin(\theta_i - \theta_j))^2$ is nonzero for $n \neq 0$ and $m \neq 0$.

The torque balance equations for all links is expressed in matrix form as

$$\mathbf{J}\ddot{\theta} = \mathbf{D}^T\mathbf{u} - l\mathbf{S}_\theta\mathbf{A}^T\mathbf{h}_x + l\mathbf{C}_\theta\mathbf{A}^T\mathbf{h}_y + \tau, \tag{19}$$

where τ is given from (13) [1]. What now remains is to remove the constraint forces from (19). By premultiplying (14) by $\mathbf{D}$ and solving for $\mathbf{h}_x$ and $\mathbf{h}_y$, we can write the expression for the joint constraint forces as

$$\begin{aligned} \mathbf{h}_x &= (\mathbf{D}\mathbf{D}^T)^{-1}\mathbf{D}(m\ddot{\mathbf{X}} + \mu_n(\mathbf{S}_\theta)^2\ddot{\mathbf{X}} - \mu_n\mathbf{S}_\theta\mathbf{C}_\theta\ddot{\mathbf{Y}} \\ &\quad - \mu_n\mathbf{S}_\theta\mathbf{C}_\theta\mathbf{V}_x^a\dot{\theta} - \mu_n(\mathbf{S}_\theta)^2\mathbf{V}_y^a\dot{\theta} - \mathbf{f^I_{D_x}} - \mathbf{f^{II}_{D_x}}) \\ \mathbf{h}_y &= (\mathbf{D}\mathbf{D}^T)^{-1}\mathbf{D}(m\ddot{\mathbf{Y}} - \mu_n\mathbf{S}_\theta\mathbf{C}_\theta\ddot{\mathbf{X}} + \mu_n(\mathbf{C}_\theta)^2\ddot{\mathbf{Y}} \\ &\quad + \mu_n(\mathbf{C}_\theta)^2\mathbf{V}_x^a\dot{\theta} + \mu_n\mathbf{S}_\theta\mathbf{C}_\theta\mathbf{V}_y^a\dot{\theta} - \mathbf{f^I_{D_y}} - \mathbf{f^{II}_{D_y}}). \end{aligned} \tag{20}$$

Inserting in (19) the joint constraints forces (20) and also replacing $\mathbf{D}\ddot{\mathbf{X}}$, $\mathbf{D}\ddot{\mathbf{Y}}$ with (15), $\ddot{\mathbf{X}}$,$\ddot{\mathbf{Y}}$ with (7) and $\ddot{p}_x$, $\ddot{p}_y$ with (17), and solving for $\ddot{\theta}$, we can finally express the model of an underwater snake robot as

$$\mathbf{M}_\theta\ddot{\theta} + \mathbf{W}_\theta\dot{\theta}^2 + \mathbf{V}_\theta\dot{\theta} + \Lambda_3|\dot{\theta}|\dot{\theta} + \mathbf{K_{Dx}}\mathbf{f_{Dx}} + \mathbf{K_{Dy}}\mathbf{f_{Dy}} = \mathbf{D}^T\mathbf{u}, \tag{21}$$

where $\mathbf{M}_\theta$, $\mathbf{W}_\theta$, $\mathbf{V}_\theta$, $\mathbf{K_{Dx}}$ and $\mathbf{K_{Dy}}$ are defined as

$$\mathbf{M}_\theta = \mathbf{J} + ml^2\mathbf{S}_\theta\mathbf{V}\mathbf{S}_\theta + ml^2\mathbf{C}_\theta\mathbf{V}\mathbf{C}_\theta + \Lambda_1 + l^2\mu_n\mathbf{K}_1\mathbf{K}^T\mathbf{S}_\theta + l^2\mu_n\mathbf{K}_2\mathbf{K}^T\mathbf{C}_\theta \tag{22}$$

$$\mathbf{W}_\theta = ml^2\mathbf{S}_\theta\mathbf{V}\mathbf{C}_\theta - ml^2\mathbf{C}_\theta\mathbf{V}\mathbf{S}_\theta + l^2\mu_n\mathbf{K}_1\mathbf{K}^T\mathbf{C}_\theta - l^2\mu_n\mathbf{K}_2\mathbf{K}^T\mathbf{S}_\theta \tag{23}$$

$$\mathbf{V}_\theta = \Lambda_2 - l\mu_n\mathbf{K}_2\mathbf{V}_x^a - l\mu_n\mathbf{K}_1\mathbf{V}_y^a \tag{24}$$

$$\mathbf{K_{Dx}} = l\mu_n m_{11}A_1\mathbf{e}\mathbf{e}^T - l\mu_n m_{21}A_2\mathbf{e}\mathbf{e}^T - l\mathbf{S}_\theta\mathbf{K} \tag{25}$$

$$\mathbf{K_{Dy}} = l\mu_n m_{12}A_1\mathbf{e}\mathbf{e}^T - l\mu_n m_{22}A_2\mathbf{e}\mathbf{e}^T + l\mathbf{C}_\theta\mathbf{K} \tag{26}$$

where $\mathbf{K}_1 = \mathbf{A}_1 + \mu_n\mathbf{A}_1\mathbf{e}\mathbf{e}^T(m_{12}\mathbf{S}_\theta\mathbf{C}_\theta - m_{11}\mathbf{S}_\theta^2) - \mu_n\mathbf{A}_2\mathbf{e}\mathbf{e}^T(m_{22}\mathbf{S}_\theta\mathbf{C}_\theta - m_{21}\mathbf{S}_\theta^2)$, $\mathbf{K}_2 = \mathbf{A}_2 - \mu_n\mathbf{A}_1\mathbf{e}\mathbf{e}^T(m_{11}\mathbf{S}_\theta\mathbf{C}_\theta - m_{12}\mathbf{C}_\theta^2) + \mu_n\mathbf{A}_2\mathbf{e}\mathbf{e}^T(m_{21}\mathbf{S}_\theta\mathbf{C}_\theta - m_{22}\mathbf{C}_\theta^2)$, $\mathbf{A}_1 = \mathbf{S}_\theta\mathbf{K}\mathbf{S}_\theta^2 + \mathbf{C}_\theta\mathbf{K}\mathbf{S}_\theta\mathbf{C}_\theta$, $\mathbf{A}_2 = \mathbf{S}_\theta\mathbf{K}\mathbf{S}_\theta\mathbf{C}_\theta + \mathbf{C}_\theta\mathbf{K}\mathbf{C}_\theta^2$.

Remark 1: The model (17,21) has been adjusted compared to the model in [1] by redefining the expression of the link accelerations as in (7) in order to avoid a singularity issue of the model presented in [1].

In summary, the equations of motion for the underwater snake robot are given by (17) and (21). By introducing the state variable $\mathbf{x} = \left[\theta^T, \mathbf{p}_{CM}^T, \dot{\theta}^T, \dot{\mathbf{p}}_{CM}^T\right]^T \in \mathbb{R}^{2n+4}$, we can rewrite the model of the robot compactly in state space form as

$$\dot{\mathbf{x}} = \left[\dot{\theta}^T, \dot{\mathbf{p}}_{CM}^T, \ddot{\theta}^T, \ddot{\mathbf{p}}_{CM}^T\right]^T = \mathbf{F}(\mathbf{x}, \mathbf{u}) \tag{27}$$

where the elements of $\mathbf{F}(\mathbf{x}, \mathbf{u})$ are found by solving (17) and (21) for $\ddot{\mathbf{p}}_{CM}$ and $\ddot{\theta}$, respectively.

III. Integral LOS Path Following Control

In this section we propose an integral line-of-sight path following control scheme for underwater snake robots. The controller consists of three main components. The first component is the gait pattern controller, which produces a sinusoidal motion pattern which propels the robot forward. The second component is the heading controller, which steers the robot towards and subsequently along the desired path. The third component is the integral LOS guidance law, which generates the desired heading angle in order to follow the desired path. An inner loop PD controller is used to control the joint angles ϕ, while an outer loop controller is used for generating the reference joint angles in order to achieve the desired sinusoidal gait pattern and also the desired heading θ_{ref} (Fig. 2). The three components of the path following controller will be presented in the following subsections.

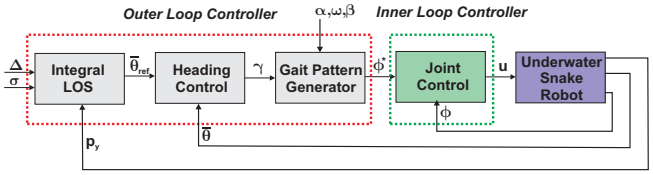

Fig. 2: Controller Structure

A. Control Objective

The path following control objective is to make the robot converge to the desired straight line path and subsequently progress along the path at some nonzero forward velocity $\bar{v}_t > 0$, where $\bar{v}_t$ is defined in (3). We consider it as less important to accurately control the forward velocity of the robot. The global x axis is aligned with the desired path, and thus the position of the robot along the global y axis corresponds to the cross track error, and the heading of the robot (1) is the angle that the robot forms with the desired path (Fig. 3). The objectives of the control system can be formalized as

$$\lim_{t\to\infty} p_y = 0 \tag{28}$$

$$\lim_{t\to\infty} \bar{\theta} = \bar{\theta}_{ss} \tag{29}$$

$$\lim_{t\to\infty} \bar{v}_t > 0 \tag{30}$$

where $\bar{\theta}_{ss}$ is a constant value which will be non-zero when the underwater snake robot is subjected to ocean currents that have a component in the transverse direction of the path. Note that since underwater snake robots having an oscillatory gait pattern the control objectives imply that p_y and $\bar{\theta}$ should have steady state oscillations about zero and $\bar{\theta}_{ss}$, respectively.

Remark 2: Note that the heading of the robot is not required to oscillate around zero but rather to oscillate around a steady-state constant value (29) in the presence of ocean currents in the transverse direction of the path. This is similar to the results shown in [20] for autonomous surface vessels. In particular, the underwater snake robot then needs to keep a nonzero heading angle in steady state in order to compensate for the current effect. A non-zero angle will allow the underwater snake robot to side-slip in order to compensate for the current effects and thus stay on the desired path, as shown in Fig. 4.

Remark 3: The current should be bounded with a constant $V_{max} > 0$ such that $V_{max} > \sqrt{V_{x,i}^2 + V_{y,i}^2}$, where $[V_{x,i}, V_{y,i}]^T$ is the current velocity expressed in inertial frame coordinates. Note that the value of V_{max} that the robot is able to compensate is directly connected to the physical limitations of the robot and the number of the links.

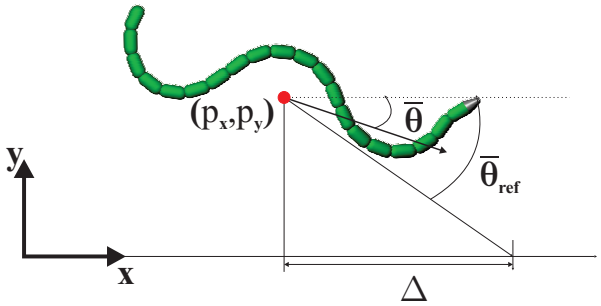

Fig. 3: The Integral LOS guidance law

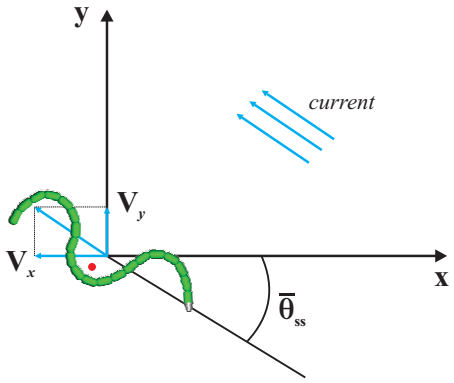

Fig. 4: Steady state: The underwater snake robot side-slips with a constant $\bar{\theta}_{ss}$ to follow the path

B. Motion Pattern

Previous studies on swimming snake robots have been focused on two motion patterns; lateral undulation and eel-like motion. In this paper we will use a general sinusoidal motion pattern that describes a broader class of motion patterns including lateral undulation and eel-like motion. Lateral undulation [2], which is the fastest and most common form of ground snake locomotion, can be achieved by creating continuous body waves, with a constant amplitude, that are propagated backwards from head to tail. In order to achieve lateral undulation, the snake robot is commanded to follow the serpenoid curve as proposed in [4]. Eel-like motion can be achieved by propagating lateral axial undulations with increasing amplitude from head to tail [7]. In this paper, a general sinusoidal motion pattern is achieved by making each joint $i \in \{1, \cdots, N-1\}$ of the underwater snake robot track the sinusoidal reference signal

$$\phi_i^*(t) = \alpha g(i,n) \sin(\omega t + (i-1)\delta) + \gamma, \tag{31}$$

where α and ω are the maximum amplitude and the frequency, respectively, δ determines the phase shift between the joints, while the function $g(i,n)$ is a scaling function for the amplitude of joint i which allows (31) to describe a quite general class of sinusoidal functions, including several different snake motion patterns. For instance, $g(i,n) = 1$ gives lateral undulation, while $g(i,n) = (n-i)/(n+1)$ gives eel-like motion [1]. The parameter γ is a joint offset coordinate

that we will use to control the direction of the locomotion [2], [22]. In particular, in [2] and [22], γ is shown to affect the direction of locomotion in the case of land-based snake robots and fish robots, respectively.

C. Outer-Loop Controller

In previous approaches the parameters α and δ are typically fixed and the parameters ω, γ are used to control the speed and the direction of the snake robot [23], [2], [22]. In this paper, the same idea will be used in order to steer the underwater snake robot to a desired orientation. In particular, the outer-loop controller will be responsible for generating the reference joint angles in order to ensure that the desired orientation is achieved. The orientation $\bar{\theta}$ of the robot is given by Eq. (1). Motivated by [19], [20] we propose to define the reference orientation using the following integral line-of-sight guidance law

$$\bar{\theta}_{\text{ref}} = -\arctan\left(\frac{p_y + \sigma y_{int}}{\Delta}\right), \qquad \Delta > 0 \tag{32}$$

$$\dot{y}_{int} = \frac{\Delta p_y}{(p_y + \sigma y_{int})^2 + \Delta^2} \tag{33}$$

where p_y is the cross-track error (i.e., the position of the underwater snake robot along the global y axis), while Δ and $\sigma > 0$ are both constant design parameters and y_{int} illustrates the integral action of the guidance law. In particular, Δ denotes the *look-ahead distance* that influences the rate of convergence to the desired path [24] and $\sigma > 0$ is the integral gain. The proposed integral LOS path following controller is commonly used for path following control of marine surface vessels in presence of unknown constant irrotational ocean current [19], [20]. The conjecture is that this choice of orientation reference will make the snake robot converge to the path, i.e. make p_y converge to zero, cf. Fig. 3.

Remark 4: The *look-ahead distance* Δ is an important design parameter that directly influences the transient motion of the underwater snake robot. Choosing Δ large should result in a well-damped transient motion, but the rate of convergence to the path will be slow, cf. Fig. 3. On the other hand, choosing Δ too small should result in poor performance or even instability. A rule of thumb is to choose Δ larger than twice the length of the robot (see e.g. [24]).

Remark 5: The integral effect becomes significant when the ocean current effect pushes the underwater snake robot away from its path. Note that (33) is designed such that the integral action has less influence when the robot is far from the path, reducing the risk of wind-up effects [20]. In fact, (32,33) behaves as a traditional LOS law when the underwater snake robot is far away from the path while the integral action takes over when the motion is closer to the desired path.

Motivated by results for ground snake robots, we seek to use the parameter γ to control the direction of the locomotion of the robot. In particular, to steer the heading $\bar{\theta}$ according to the integral LOS angle in (32), we choose the joint angle offset according to

$$\gamma = k_\theta \left(\bar{\theta} - \bar{\theta}_{\text{ref}}\right), \tag{34}$$

where $k_\theta > 0$ is a control gain [2].

D. Inner-loop controller

In order to make the joint angle ϕ_i follows its reference signal ϕ_i^*, a PD controller is used:

$$u_i = k_p(\phi_i^* - \phi_i) + k_d(\dot{\phi}_i^* - \dot{\phi}_i), \quad i = 1, \ldots, n-1, \tag{35}$$

where $k_p > 0$ and $k_d > 0$ are the gains of the controller.

IV. Stability analysis of the integral LOS path following controller based on the Poincaré map

In this section, the theory of Poincaré maps is employed to prove that the integral LOS path following controller proposed in Section III generates a locally exponentially stable periodic orbit in the state space of the underwater snake robot. This periodic orbit implies that the robot locomotes along the desired straight path in the presence of current.

A. The Poincaré map

The Poincaré map is a useful tool for studying the stability of periodic solutions in dynamical systems [25]. In particular, the stability of a periodic orbit of a dynamical system is related to the stability of the fixed point of the corresponding Poincaré map of the system. We will thus use a Poincaré map approach as a stability analysis tool for the closed-loop system of an underwater snake robot with the path following controller presented in Section III. In particular, the exponential stability of the system will be investigated by checking if the fixed point is an exponentially stable equilibrium point of the discrete system. The fixed point $\bar{\mathbf{x}}^*$ is locally exponentially stable if the magnitudes of all the eigenvalues of the Jacobian linearization of the Poincaré map $\mathbf{J}_P(\bar{\mathbf{x}}^*)$ about the fixed point are strictly less than one.

Note that in order to investigate the stability properties using Poincaré maps, the model of the underwater snake robot should be represented as an autonomous system. Following the approach described in [26], the model (27) with the path following controller proposed in Section III can be rewritten as the following autonomous system

$$\begin{aligned} \dot{\mathbf{x}} &= \mathbf{F}\left(\mathbf{x}, \frac{T}{2\pi}\beta\right), \qquad \mathbf{x}(t_0) = \mathbf{x}_0 \\ \dot{\beta} &= \frac{2\pi}{T}, \qquad \beta(t_0) = \frac{2\pi t_0}{T} \end{aligned} \tag{36}$$

where $\beta = 2\pi t/T$ is a new state variable and $T = 2\pi/\omega$ is the period of the cyclic locomotion generated by the sinusoidal gait pattern in (31). The state variable β is periodic since we force β to be $0 \leq \beta < 2\pi$, i.e. we set β to zero each time $\beta = 2\pi$.

What now remains is to specify the Poincaré section for the underwater snake robot. We choose the global x axis as the Poincaré section S of the system in (36) (see e.g. [2]). Furthermore, we exclude p_x from the Poincaré map since the forward position of the robot will not undergo limit cycle behaviour like the other states of the system. As a result, the Poincaré section is given by $S = \{(\theta, p_y, \dot{\theta}, \beta) | p_y = 0\}$, which means that the vector of the independent time-periodic states constrained to S can be expressed as $\bar{x} = \left[\theta^T, \dot{\theta}^T, \dot{\mathbf{p}}_{CM}^T, \beta\right]^T \in \mathbb{R}^{2n+3}$.

Remark 6: Note that since p_x is not present on the right hand side in any of the dynamic equations in (27), we can exclude

p_x from the Poincaré map without affecting the other state variables of the system (27).

Remark 7: In this paper we consider a one-sided Poincaré map by assuming that the Poincaré section is crossed when the CM position of the underwater snake robot crosses the x axis from above, similar to the approach presented in [2], [21] for ground snake robots.

B. Stability analysis of the Poincaré map

In order to investigate the stability of the robot with the integral LOS path following controller proposed in Section III, we consider an underwater snake robot with $n = 3$ links, each one having length $2l = 0.14$ m and mass $m = 0.6597$ kg. The hydrodynamic parameters are $c_t = 0.2639$, $c_n = 8.4$, $\mu_n = 0.3958$, $\lambda_1 = 2.298810^{-7}$, $\lambda_2 = 4.310310^{-4}$ and $\lambda_3 = 2.262910^{-5}$. An extensive discussion about the values of the fluid parameters can be found in [1]. The values of a constant ocean current in the inertial frame are $[0.005, 0.01]$ m/sec. The joint PD controller (35) is used for each joint with parameters $k_p = 20$, $k_d = 5$, and lateral undulation and eel-like motion are achieved by choosing $\mathrm{g}(i,n) = 1$ and $\mathrm{g}(i,n) = (n-i)/(n+1)$, respectively, with gait parameters $\alpha = 70^\mathrm{o}$, $\delta = 70^\mathrm{o}$ and $\omega = 120^\mathrm{o}/\mathrm{s}$ in (31). Initially, we run simulations with the proposed control strategy until the robot reaches the desired path, and then we choose the initial values of y_{int} as 5.33 and 6.54 for lateral undulation and eel-like motion, respectively. Note that these initial values are used for the stability analysis of the system by using Poincaré map. Furthermore, the control gain in (34) is $k_\theta = 0.8$, while the guidance law parameters in (32-33) are chosen as $\Delta = 2ln$ [24], and $\sigma = 0.01$ [20].

The Poincaré map of the underwater snake robot model in (17,21) found using Matlab R2011b. The dynamics is calculated using the ode23tb solver with a relative and absolute error tolerance of 10^{-4}. Using the Newton-Raphson algorithm the fixed point, $\bar{\mathbf{x}}^* \in \mathbb{R}^9$, of the Poincaré map for lateral undulation and eel-like motion are given by (37) and (38), respectively.

$$\begin{aligned}\bar{\mathbf{x}}^* = [&-35.06^\mathrm{o}, -41.79^\mathrm{o}, 17.68^\mathrm{o}, -108.83^\mathrm{o}/\mathrm{s}, 26.49^\mathrm{o}/\mathrm{s},\\ &106.96^\mathrm{o}/\mathrm{s}, 10.59\mathrm{cm}/\mathrm{s}, -3.86\mathrm{cm}/\mathrm{s}, 194.04^\mathrm{o}]^T\end{aligned} \tag{37}$$

$$\begin{aligned}\bar{\mathbf{x}}^* = [&-15.77^\mathrm{o}, -29.99^\mathrm{o}, -2.21^\mathrm{o}, -116.75^\mathrm{o}/\mathrm{s},\\ &20.62^\mathrm{o}/\mathrm{s}, 70.89^\mathrm{o}/\mathrm{s}, 9.10\mathrm{cm}/\mathrm{s}, -1.57\mathrm{cm}/\mathrm{s}, 191.88^\mathrm{o}]^T\end{aligned} \tag{38}$$

The locomotion of the robot over one period is shown in Fig. 5 and 6 for lateral undulation and eel-like motion, respectively. The initial values of the states of the robot are given by (37) and (38), and the initial position is chosen as $\mathbf{p}_{\mathrm{CM}} = 0$. From Fig. 5 and 6, we can see that after one period of the motion the state variables have returned to their initial values given by (37) and (38). In addition, after one period of motion the position of the robot along the x axis has increased. Furthermore, Fig. 7a and 8a illustrate the limit cycle that is traced out by the three link angles of the robot for lateral undulation and eel-like motion. The Jacobian linearization of the Poincaré map about the fixed points (37) and (38) are calculated, and the magnitudes of

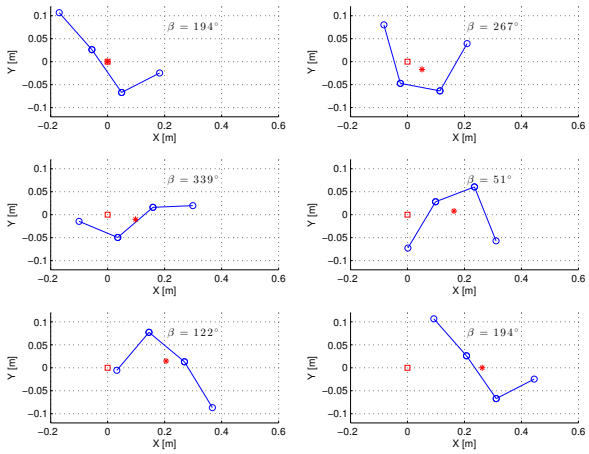

Fig. 5: Motion of the underwater snake for lateral undulation

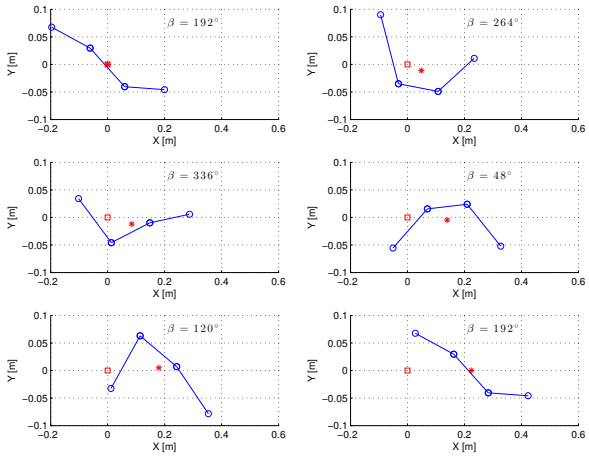

Fig. 6: Motion of the underwater snake for eel-like motion

the eigenvalues of $\mathbf{J}_P(\bar{\mathbf{x}}^*) \in \mathbb{R}^{9\times 9}$ are found to be given by (39) and (40) for lateral undulation and eel-like motion, respectively:

$$\begin{aligned}|\,\mathrm{eig}(\mathbf{J}_P(\bar{\mathbf{x}}^*))\,| = [&0.394, 0.394, 0.041, 0.008, 0.002,\\ &0.002, 2.82\times 10^{-4}, 2.82\times 10^{-4}, 4.84\times 10^{-5}]^T\end{aligned} \tag{39}$$

$$\begin{aligned}|\,\mathrm{eig}(\mathbf{J}_P(\bar{\mathbf{x}}^*))\,| = [&0.548, 0.548, 0.059, 0.059, 0.011,\\ &1.49\times 10^{-3}, 2.92\times 10^{-4}, 1.02\times 10^{-4}, 9.25\times 10^{-5}]^T\end{aligned} \tag{40}$$

From (39) and (40), it is easily seen that all the eigenvalues, both for lateral undulation and eel-like motion cases, are strictly less than one. Therefore we can conclude that the periodic orbit is locally exponentially stable for the given choice of controller parameters both for lateral undulation and eel-like motion. Since the periodic orbit is exponentially stable and the system returns to $p_y = 0$ with time period T, we can conclude that the control objective (28) is achieved. Furthermore, in [27] it is shown that for an underwater snake robot under anisotropic drag effects propulsive forces are positive as long as $\mathrm{sgn}(\theta_i) = \mathrm{sgn}(\dot{y}_i)$ and $\mathrm{sgn}(\theta_i) = \mathrm{sgn}(\ddot{y}_i)$. Fig. 7b-7c and 8b-8c show that these conditions are valid over the majority of the period for both lateral undulation and eel-like motion. Hence the robot moves forward and the control objective (30) is satisfied. Since the control objectives (28) and (30) are both satisfied, we can argue that the control

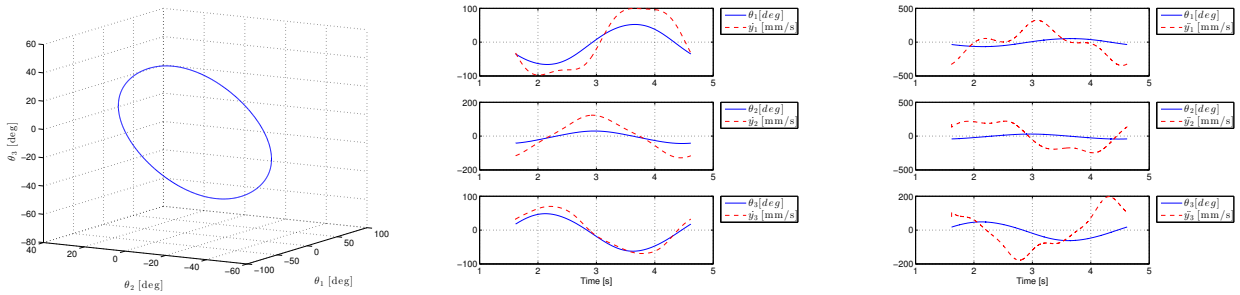

(a) The limit cycle (b) Plot of θ_i and $\dot{y}_i$ (c) Plot of θ_i and $\ddot{y}_i$

Fig. 7: Stability analysis of the Poincaré map for lateral undulation

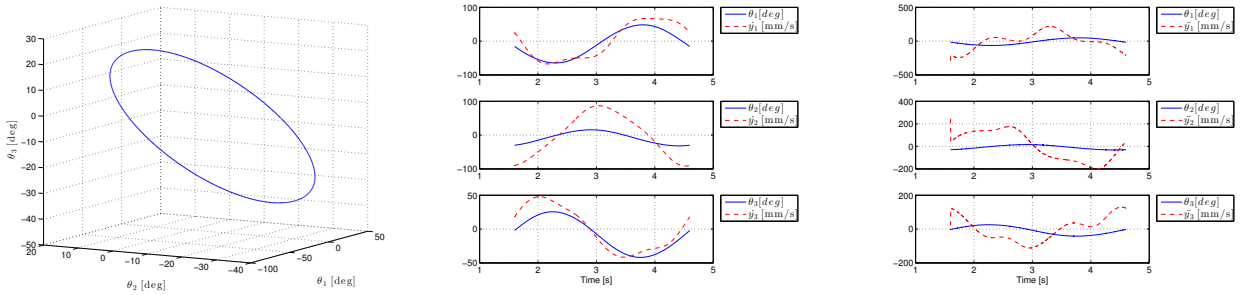

(a) The limit cycle (b) Plot of θ_i and $\dot{y}_i$ (c) Plot of θ_i and $\ddot{y}_i$

Fig. 8: Stability analysis of the Poincaré map for eel-like motion

objective (29) must be satisfied. Note that if the heading did not oscillate around $\bar{\theta}_{ss}$, but rather around zero, then the robot would not be able to compensate the ocean current effects and the robot would drift away from the desired path, which contradicts the fulfilment of control objective (28).

Remark 8: A more formal stability analysis of the system in (17,21) with the proposed controller remains a challenging task, mainly due to the complexity of the dynamic system equations [1]. Thus a numerical approach is adopted in this paper. Note that by using the Poincaré map approach, we have only proven that the stability of the proposed path following controller presented in Section III holds for the numerical parameters of the system presented in the beginning of this subsection. However, simulations indicate that the proposed path following controller can be applied to steer the robot to the desired path in the presence of ocean currents for other parameters of the system and for a wide range of the current values.

V. Simulation Study

This section presents simulation results in order to investigate the performance of the integral line-of-sight path following controller described in Section III. The model and controller parameters are the same as in Section IV. The initial values of all states of the robot are set to zero except for the initial position of the center of mass, which is selected as $p_{CM}(0) = [0, 0.5]$. In Fig. 9a and Fig. 10a we can see that (34) makes the heading angle converge to and oscillate about the desired heading angle given by (32) for lateral undulation and eel-like motion, respectively. Note that the heading of the robot does not converge to oscillations about zero but rather converges to a steady state constant value, $\bar{\theta}_{ss}$, which means that the control objective (29) is achieved. Moreover, Fig. 9b and Fig. 10b show that control objective (28) is verified, i.e. the integral LOS guidance law (32) will make the cross track error converge to zero. Finally, from Fig. 9c and Fig. 10c we can see that the CM of the underwater snake robot converges to the desired path for both lateral undulation and eel-like motion. Fig. 9-10 clearly shows that the heading, the cross track error and the position of the robot have a steady state oscillatory behavior when the robot reaches the desired path, as it has been predicted in Section III.A.

VI. Conclusions

This paper has proposed an integral line-of-sight path following controller for underwater snake robots. In particular, a straight line path following controller for an underwater snake robot in the presence of constant irrotational currents was proposed. The integral line-of-sight guidance law was combined with a directional controller to steer the robot to the path, where integral action was introduced to compensate for the effect of ocean currents. It was shown that the integral LOS guidance law can be applied to underwater snake robots to compensate for the current effect and achieve path following of straight lines. In addition, the stability of the locomotion along the straight line path in the presence of current was analysed. By use of a Poincaré map, we proved that all state variables of an underwater snake robot, except the position along the forward direction, trace out an exponentially stable periodic orbit when the integral LOS path following controller is applied. Simulation results illustrated the performance of the proposed control strategy.

References

[1] E. Kelasidi, K. Y. Pettersen, J. T. Gravdahl, and P. Liljebäck, "Modeling of underwater snake robots," in *Proc. IEEE International*

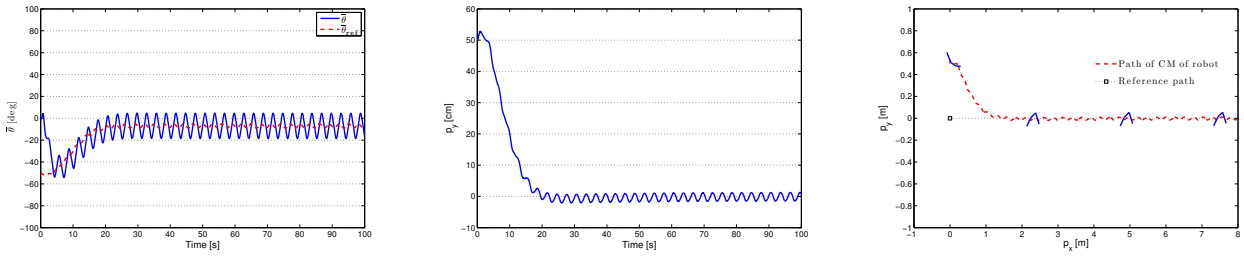

(a) Heading angle (b) Cross track error (c) Path of the robot

Fig. 9: Integral LOS path following controller for lateral undulation

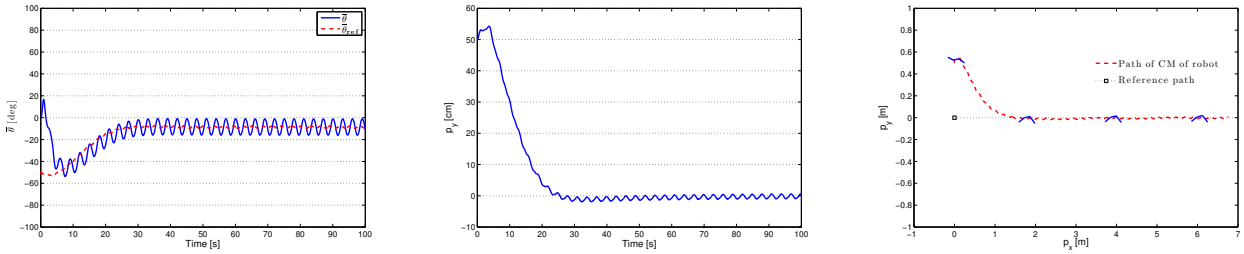

(a) Heading angle (b) Cross track error (c) Path of the robot

Fig. 10: Integral LOS path following controller for eel-like motion

Conference on Robotics and Automation (ICRA), Hong Kong, China, May 31 - June 7 2014.

[2] P. Liljebäck, K. Y. Pettersen, Ø. Stavdahl, and J. T. Gravdahl, *Snake Robots: Modelling, Mechatronics, and Control*. Springer-Verlag, Advances in Industrial Control, 2013.

[3] J. Gray, "Studies in animal locomotion," *Journal of Experimental Biology*, vol. 10, no. 1, pp. 88–104, 1933.

[4] S. Hirose, *Biologically Inspired Robots: Snake-Like Locomotors and Manipulators*. Oxford: Oxford University Press, 1993.

[5] A. Crespi, A. Badertscher, A. Guignard, and A. Ijspeert, "Swimming and crawling with an amphibious snake robot," in *Proc. IEEE International Conference on Robotics and Automation (ICRA).*, April 2005, pp. 3024 – 3028.

[6] H. Yamada, S. Chigisaki, M. Mori, K.Takita, K. Ogami, and S. Hirose, "Development of amphibious snake-like robot ACM-R5," in *36th International Symposium on Robotics*, Tokyo, Japan, November 29-December 1 2005.

[7] J. Colgate and K. Lynch, "Mechanics and control of swimming: a review," *IEEE Journal of Oceanic Engineering*, vol. 29, no. 3, pp. 660 – 673, July 2004.

[8] K. McIsaac and J. Ostrowski, "Motion planning for anguilliform locomotion," *IEEE Transactions on Robotics and Automation*, vol. 19, no. 4, pp. 637–625, 2003.

[9] F. Boyer, M. Porez, and W. Khalil, "Macro-continuous computed torque algorithm for a three-dimensional eel-like robot," *IEEE Transactions on Robotics*, vol. 22, no. 4, pp. 763 –775, aug. 2006.

[10] G. Taylor, "Analysis of the swimming of long and narrow animals," *Proceedings of the Royal Society of London. Series A. Mathematical and Physical Sciences*, vol. 214, no. 1117, pp. 158–183, 1952.

[11] M. J. Lighthill, "Large-amplitude elongated-body theory of fish locomotion," *Proceedings of the Royal Society of London. Series B. Biological Sciences*, vol. 179, no. 1055, pp. 125–138, 1971.

[12] J. Chen, W. O. Friesen, and T. Iwasaki, "Mechanisms underlying rhythmic locomotion: bodyfluid interaction in undulatory swimming," *The Journal of Experimental Biology*, vol. 214, no. 4, pp. 561–574, 2011.

[13] A. Wiens and M. Nahon, "Optimally efficient swimming in hyper-redundant mechanisms: control, design, and energy recovery." *Bioinspir Biomim*, vol. 7, no. 4, p. 046016, 2012.

[14] W. Khalil, G. Gallot, and F. Boyer, "Dynamic modeling and simulation of a 3-D serial eel-like robot," *IEEE Transactions on Systems, Man, and Cybernetics, Part C: Applications and Reviews*, vol. 37, no. 6, pp. 1259 –1268, Nov. 2007.

[15] P. A. Vela, K. A. Morgansen, and J. W. Burdick, "Underwater locomotion from oscillatory shape deformations," in *Proc. IEEE Conf. Decision and Control*, vol. 2, Dec. 2002, pp. 2074–2080.

[16] K. Morgansen, B. Triplett, and D. Klein, "Geometric methods for modeling and control of free-swimming fin-actuated underwater vehicles," *IEEE Transactions on Robotics*, vol. 23, no. 6, pp. 1184 –1199, Dec. 2007.

[17] A. Crespi and A. J. Ijspeert, "AmphiBot II: An Amphibious Snake Robot that Crawls and Swims using a Central Pattern Generator," in *Proc. 9th International Conference on Climbing and Walking Robots (CLAWAR)*, September 2006, pp. 19–27.

[18] K. A. McIsaac and J. P. Ostrowski, "A framework for steering dynamic robotic locomotion systems," *Int. J. Robot. Res.*, vol. 22, no. 2, pp. 83–97, February 2003.

[19] E. Borhaug, A. Pavlov, and K. Pettersen, "Integral los control for path following of underactuated marine surface vessels in the presence of constant ocean currents," in *47th IEEE Conference on Decision and Control (CDC)*, Dec 2008, pp. 4984–4991.

[20] W. Caharija, K. Y. Pettersen, A. Sorensen, M. Candeloro, and J. T. Gravdahl, "Relative velocity control and integral line of sight for path following of autonomous surface vessels: Merging intuition with theory," *Proceedings of the Institution of Mechanical Engineers, Part M: Journal of Engineering for the Maritime Environment*, Dec 2013.

[21] P. Liljeback, K. Pettersen, O. Stavdahl, and J. Gravdahl, "Controllability and stability analysis of planar snake robot locomotion," *IEEE Transactions on Automatic Control*, vol. 56, no. 6, pp. 1365–1380, June 2011.

[22] J. Guo, "A waypoint-tracking controller for a biomimetic autonomous underwater vehicle," *Ocean Engineering*, vol. 33, pp. 2369 – 2380, 2006.

[23] E. Kelasidi and A. Tzes, "Serpentine motion control of snake robots for curvature and heading based trajectory - parameterization," in *Proc. 20th Mediterranean Conference on Control Automation (MED)*, 2012, pp. 536–541.

[24] T. I. Fossen, *Handbook of Marine Craft Hydrodynamics and Motion Control*. John Wiley & Sons, Ltd, 2011.

[25] H. K. Khalil, *Nonlinear Systems*, 3rd ed. Prentice Hall, Ed., 2002.

[26] T. Parker and L. Chua, *Practical numerical algorithms for chaotic systems*. Berlin: Springer Verlag, 1989.

[27] E. Kelasidi, K. Y. Pettersen, and J. T. Gravdahl, "A control-oriented model of underwater snake robots," in *Proc. IEEE International Conference on Robotics and Biomimetics*, Bali, Indonesia, Dec. 5-10 2014, (Submitted). [Online]. Available: https://www.dropbox.com/s/jkea1ddorctmcn7/ROBIO2014.pdf